



HAL
open science

Influence of the alloy microstructure and surface state on the protective properties of trivalent chromium coatings grown on a 2024 aluminium alloy

Xavier Verdalet-Guardiola, Jean-Pierre Bonino, Sandrine Nathalie Duluard, Benoit Fori, Christine Blanc

► To cite this version:

Xavier Verdalet-Guardiola, Jean-Pierre Bonino, Sandrine Nathalie Duluard, Benoit Fori, Christine Blanc. Influence of the alloy microstructure and surface state on the protective properties of trivalent chromium coatings grown on a 2024 aluminium alloy. *Surface and Coatings Technology*, 2018, 344, pp.276-287. 10.1016/j.surfcoat.2018.03.046 . hal-01989083

HAL Id: hal-01989083

<https://hal.science/hal-01989083>

Submitted on 22 Jan 2019

HAL is a multi-disciplinary open access archive for the deposit and dissemination of scientific research documents, whether they are published or not. The documents may come from teaching and research institutions in France or abroad, or from public or private research centers.

L'archive ouverte pluridisciplinaire **HAL**, est destinée au dépôt et à la diffusion de documents scientifiques de niveau recherche, publiés ou non, émanant des établissements d'enseignement et de recherche français ou étrangers, des laboratoires publics ou privés.



Open Archive Toulouse Archive Ouverte (OATAO)

OATAO is an open access repository that collects the work of Toulouse researchers and makes it freely available over the web where possible

This is an author's version published in: <http://oatao.univ-toulouse.fr/21409>

Official URL: <https://doi.org/10.1016/j.surfcoat.2018.03.046>

To cite this version:

Verdalet-Guardiola, Xavier  and Bonino, Jean-Pierre  and Duluard, Sandrine Nathalie  and Fori, Benoit and Blanc, Christine  *Influence of the alloy microstructure and surface state on the protective properties of trivalent chromium coatings grown on a 2024 aluminium alloy.* (2018) *Surface and Coatings Technology*, 344. 276-287. ISSN 0257-8972

Any correspondence concerning this service should be sent to the repository administrator: tech-oatao@listes-diff.inp-toulouse.fr

Influence of the alloy microstructure and surface state on the protective properties of trivalent chromium coatings grown on a 2024 aluminium alloy

Xavier Verdalet-Guardiola^{a,b,c}, Jean-Pierre Bonino^b, Sandrine Duluard^b, Benoit Fori^c,
Christine Blanc^{a,*}

^a CIRIMAT, Université de Toulouse, CNRS, ENSIACET, 4 allée Emile Monso, BP 44362, 31030 Toulouse cedex 4, France

^b CIRIMAT, Université de Toulouse, CNRS, UPS, 118 route de Narbonne, 31062 Toulouse cedex 9, France

^c MECAPROTEC Industries, 34 Boulevard de Joffrery, BP 30204, 31605 Muret Cedex, France

ARTICLE INFO

Keywords:

Trivalent chromium coating
Aluminium alloy
Protective properties
Copper
Microstructure
Electrochemical impedance spectroscopy

ABSTRACT

The protective properties of trivalent chromium process (TCP) coatings grown on a 2024-T3 aluminium alloy were studied on the basis of electrochemical measurements performed both in sulphate and chloride solutions and neutral salt spray tests. The influence of the alloy microstructure and surface state was studied: two batches, each one characterized by its own coarse intermetallic particle distribution, and two surface states, i.e. laminated and polished, were considered. Results showed that in 0.1 M Na₂SO₄, the protective properties of the TCP coatings decreased when the roughness of the initial surface increased. Furthermore, improved protective properties were observed for a TCP coating grown on a surface containing a lower amount of Al-Cu-Mg IMCs in the initial microstructure. The most plausible explanation is that a fast kinetics of coating growth, either associated to strong initial roughness or a great surface copper coverage, was detrimental for the protective properties of the coatings. In more aggressive solutions, i.e. 0.5 M NaCl solution or for neutral salt spray tests, the differences are not significant. The findings are highly relevant for industrial applications: the results showed that variations in batches, for a same type of alloy, or in initial surface state should not be detrimental for the corrosion resistance of the TCP coated samples. However, the conversion process had to be adapted for different types of alloys, characterized by their own microstructure.

1. Introduction

Aluminium alloys are widely used in the aeronautical industry due to their high specific modulus E/ρ (E , Young modulus and ρ , density) that allows the mass of the structures to be reduced [1]. Their good mechanical properties are mainly related to the addition of different alloying elements that, unfortunately, lead to a decrease of the corrosion resistance of the alloys when compared to pure aluminium [2,3]. Chromate conversion coatings were largely used to improve the corrosion resistance of aluminium alloys. However, European regulation REACH, that bans the use of hexavalent chromium, will become effective in 2024 [4]. Therefore, new chemical conversion treatments are developed. Trivalent chromium processes (TCP) constitute one of the most promising substitution solutions [5–9].

Contrary to chromate coatings, anti-corrosion properties of trivalent chromium coatings are known to depend significantly on the surface preparation, i.e. pre-treatments performed before TCP [2,7,10–17]. Before chemical conversion, the alloy surface is cleaned in a degreasing

solution to remove fats and oils. Then, a desmutting solution dissolves the native oxide and allows the formation of a new oxide with controlled thickness and composition [2]. Li et al. have shown that a long desmutting step reduces the anti-corrosion performance of a commercial trivalent chromium coating (Alodine 5900 RTU coating, Henkel group) [17]. They attributed the decrease of the anticorrosion properties to the roughness generated by the desmutting process, and more precisely, to the nucleation and growth of pits with increasing depth over the time of desmutting in Turco Liquid Smut-Go NC. Toh et al. have studied different desmutting solutions on aluminium alloy 7475-T7651; they have shown important differences in the morphology and oxide roughness at the alloy surface [18]. Others works have shown a huge influence of the substrate microstructure on the surface reactivity during the pre-treatments and as a consequence on the anti-corrosion properties of the coatings [19–22]. Considering the complex microstructure of industrial aluminium alloys, it seems difficult to establish a clear relationship between the effects of the pre-treatments on the surface morphology, the kinetics of TCP coating growth and the

* Corresponding author.

E-mail address: christine.blanc@ensiacet.fr (C. Blanc).

subsequent protective properties of the TCP coatings. All of this gave rise to new challenges at the industrial scale. The first one concerns the ability to generalize the conversion process to different alloys; the second one is related to the need to get away from the influence of the surface state of the substrate before the pre-treatments on the growth of the TCP coatings and their subsequent anticorrosion properties.

In the present work, the surface morphology, chemistry and reactivity after different steps of pre-treatment (degreasing and desmutting) were studied for three samples of AA 2024-T3: two polished samples from two batches of AA 2024-T3 to study the influence of the microstructure and a laminated sample of one of the two batches to determine, by comparison with the polished sample of the same batch, the effect of the surface state before pre-treatment. Then, the growth rate of the TCP coatings was analysed and their protective properties were evaluated by means of OCP measurements, potentiodynamic polarisation, electrochemical impedance spectroscopy measurements and neutral salt spray tests.

2. Materials and methods

2.1. Materials and sample preparation

The material used was a cold rolled AA 2024-T3 provided as sheets of different thicknesses with similar chemical compositions (Table 1). Two batches were studied and called as alloy A for the 1 mm thick sheet and alloy B for the 3 mm thick sheet respectively. All samples corresponded to $125 \times 80 \times 3 \text{ mm}^3$ parallelepipeds removed from the sheets. Alloy A was studied as received, i.e. after rolling: the samples were called as laminated samples in the following. Other samples of alloys A and B were abraded using SiC paper down to 1200 and then mechanically-polished to a $1 \mu\text{m}$ colloidal diamond finish prior to the pre-treatment. They constituted a reference surface state and are called as polished samples in the following. The samples were protected using a silicone one-component (CAF1, Bluestar Silicones) in order to expose only one side to the different solutions with a 4 (or 10) cm^2 surface area. They were rinsed with acetone prior to the pre-treatments in order to remove inks and other surface pollutants. Then, they were degreased in an alkaline bath ($40 \text{ g}\cdot\text{L}^{-1}$ sodium tripolyphosphate, $40 \text{ g}\cdot\text{L}^{-1}$ borax and $5 \text{ mL}\cdot\text{L}^{-1}$ Turco 4215 additive, $\text{pH} = 9$) for 1200 s at 60°C . Finally, they were immersed in the desmutting bath, i.e. a sulfo-nitro-ferric solution ($\text{pH} = 1$) for 300 s at room temperature. All the pre-treatment steps were followed by a rinsing in deionised water. All reactants used are of industrial quality.

For the formation of the TCP coating, the degreased and desmutted samples were first immersed for 600 s in the conversion solution (32% v/v Socosurf TCS (Socomore, France), pH between 3.8 and 4) at 40°C to form the conversion layer. The coated samples were then immersed in the post-treatment solution (10% v/v Socosurf PACS (Socomore, France), 5% v/v H_2O_2 at 35% v/v in water, pH between 4.2 and 5.3) at room temperature for 300 s. All treatments were followed by rinsing in deionised water. Finally, the samples were dried at 60°C during 600 s.

2.2. Characterisation of the surface morphology and microstructure. Morphology of the TCP coatings

Scanning Electron Microscopy – Field Emission Gun (SEM-FEG) observations were performed with a JEOL JSM 7800F Prime (platform of Micro-characterisation Raimond Castaing, Toulouse) operating at

Table 2

Classification criteria used for the identification of IMCs ($\phi > 2 \mu\text{m}$) where \bar{X} corresponds to the results of measurements performed for the matrix.

Type	Al-Cu-Mn-Fe-Si	Al-Cu-Mg	Al-Cu
Classification criteria	$\text{Fe} > \bar{F}\bar{e} + 0.2$ $\text{Cu} > \bar{C}\bar{u}$	$\text{Mg} > \bar{M}\bar{g} + 0.5$ $\text{Fe} \approx \bar{F}\bar{e}$	$\text{Mg} \approx \bar{M}\bar{g}$ $\text{Fe} \approx \bar{F}\bar{e}$ $\text{Cu} > \bar{C}\bar{u} + 1$

5 kV (secondary electrons) and 10 kV (backscattered electrons) to characterize both the surface morphology and microstructure of the alloys. Concerning the microstructure, attention was paid to coarse intermetallic particles (IMC); energy dispersive spectroscopy (EDS) measurements performed by means of a EDS SDD X-Max 80 mm^2 Oxford Instruments AZtecEnergy allowed three types of IMC ($\phi > 2 \mu\text{m}$) to be distinguished on the basis of the classification criteria described in Table 2. Transmission electron microscopy (TEM) observations were performed with a JEOL JEM 2100F (platform of Micro-characterisation Raimond Castaing, Toulouse) operating at 200 kV to characterize the structure of the TCP coatings. TEM samples were prepared with a Scanning Electron Microscopy – Focused Ion Beam FEI HELIOS 600i (platform of Micro-characterisation Raimond Castaing, Toulouse) equipped with a Gallium Ionic Canon. Samples were covered by an electronic carbon coating ($0.5 \mu\text{m}$, operating at 5 kV and 2.5 nA, precursor: Naphtalene (C_{10}H_8) and an ionic platinum coating ($3 \mu\text{m}$, operating at 30 kV and 0.43 nA, precursor: Methylcyclopentadieny(trimethyl)platinum ($\text{C}_5\text{H}_4\text{CH}_3\text{Pt}(\text{CH}_3)_3$) before cutting operating at 30 kV and 47 nA to 80 pA.

2.3. Characterisation of the electrochemical behaviour and protective properties

The reactivity of the alloy surface before and after the two pre-treatment steps, related mainly to the corrosion behaviour of the IMCs present on the sample surface, was evaluated by performing anodic polarisation in a 0.1 M Na_2SO_4 solution [23]. A three-electrode cell connected to a Bio-Logic VSP potentiostat was used with a saturated calomel electrode (SCE) as reference electrode and a graphite rod as counter electrode. The working electrode was placed vertically with a surface exposed to the electrolyte of 4 cm^2 . Polarisation was performed from open circuit potential (OCP) minus 0.05 V to 0.5 V/SCE at $500 \text{ mV}\cdot\text{h}^{-1}$ after 1 h of immersion at OCP.

The relative electroactive copper content on the sample surface (4 cm^2 exposed to the solution) was determined by cyclic voltammetry (CV) experiments performed in deaerated borate buffer solution ($8.17 \text{ g}\cdot\text{L}^{-1}$ $\text{Na}_2\text{B}_4\text{O}_7 \cdot 10 \text{ H}_2\text{O}$, $7.07 \text{ g}\cdot\text{L}^{-1}$ H_3BO_3 , $\text{pH} = 8.4$) at room temperature [16,24]. The solution was deaerated for 15 min with nitrogen bubbling before CV experiments. The procedure consisted of (a) a 5 min polarisation at $-0.7 \text{ V}_{\text{SCE}}$; (b) scan from $-0.7 \text{ V}_{\text{SCE}}$ to $0.3 \text{ V}_{\text{SCE}}$ then back to $-1.2 \text{ V}_{\text{SCE}}$ at $1 \text{ mV}\cdot\text{s}^{-1}$; (c) hold at $-0.7 \text{ V}_{\text{SCE}}$ during 10 min; (d) repeat step (b); (e) hold at $-0.7 \text{ V}_{\text{SCE}}$ during 20 min; (f) repeat step (b). The area under $\text{Cu}(0) \rightarrow \text{Cu}(I)$ peak in the last scan was used to determine the relative electroactive copper content as largely detailed in Scully's work [25,26].

Electrochemical impedance spectroscopy (EIS) measurements were performed in naturally aerated 0.1 M Na_2SO_4 solution at room temperature to evaluate the protective properties of the coatings using the

Table 1

Composition of 2024-T3 aluminium alloys.

Wt%	Al	Cu	Mg	Mn	Fe	Si	Cr	Zn	Ti	V	Zr	Other
A	Balance	4.5	1.4	0.57	0.21	0.08	0.01	0.13	0.02	0.01	0.01	0.05
B	Balance	4.4	1.4	0.51	0.15	0.08	0.01	0.17	0.02		0.01	0.05

same experimental set-up as for the polarisation experiments except for the position of the working electrode, horizontal, at the bottom of the cell in this case. The samples (surface exposed to the electrolyte of 10 cm^2) were first exposed to the solution for one hour at their corrosion potential before the first measurement (i.e. 0 day) in order to stabilise the OCP value. EIS measurements were carried out for different immersion times: 0, 3, 7, 14, 21 and 28 days. They were performed at the OCP in the frequency range 6.10^4 to 5.10^{-3} Hz with a potential amplitude of 10 mV (rms). EC-lab software (version 10.37, Bio-Logic) was used to fit the experimental EIS spectra.

To complete the EIS experiments, OCP measurements and potentiodynamic polarisations were performed in 0.5 M NaCl solution by means of the same experimental set-up than before (surface exposed to the electrolyte of 4 cm^2). For the potentiodynamic polarisations, the samples were first maintained at their OCP for 1 h and then the anodic and cathodic parts were obtained independently from the OCP - 50 mV (+50 mV for the cathodic part) at a potential sweep rate of 0.14 mV s^{-1} . Neutral salt spray tests (NSST) were achieved also in an Ascott salt spray chamber S120iS. Salt spray tests were performed under ISO9227 specification. Each sample was a parallelepiped with a 1 dm^2 surface area exposed to the electrolyte and was inspected each 24 h. In these conditions, corrosivity tests (ISO9227) for CR4 steel exhibit a corrosion rate of 68 g m^{-2} for 48 h.

All the experiments previously described were repeated three times in order to evaluate the reproducibility of the results.

2.4. Characterisation of the wettability of the surface

Water contact angle was measured with an optical tensiometer Attension Theta T200-Basic and analysed with OneAttension software (Attension Theta). Water contact angle values were recorded for 10 s and the wettability was defined from the values recorded between 8 and 10 s. The measurements were performed immediately after the different treatment steps and repeated 10 times minimum for each condition.

3. Results and discussions

3.1. Characterisation of the surface before the conversion process

3.1.1. Surface morphology for AA 2024-T3 after the pre-treatment step, i.e. degreasing and desmutting

SEM-FEG micrographs of the AA 2024-T3 surface for A and B alloys before pre-treatment (after acetone rinsing) and after each step of pre-treatment (degreasing and desmutting) are presented in Fig. 1. Before pre-treatment, laminated sample surfaces presented numerous defects related to the rolling process, i.e. rolling grooves, wrenching of mater, inclusions (Fig. 1a) while polished sample surfaces exhibited low roughness due to the mechanical polishing process (Fig. 1d and g). All the surfaces exhibited IMCs of various sizes (Fig. 2). The nature of these particles and the surface area they covered will be detailed in the next paragraph. After degreasing, all the surfaces showed a scalloped morphology and a high quantity of both residues and IMCs (Fig. 1b, e and h). After desmutting, all the samples showed a similar surface morphology characterized by a scalloped surface with fewer residues (Fig. 1c, f and i). Almost all the IMCs had been removed from the alloy surface after this pre-treatment step. For the laminated surfaces (Fig. 1c), rolling defects were still observed after surface degreasing and desmutting treatments.

The scalloped surface is characteristic of a severe chemical attack of the aluminium matrix. In the literature, such a significant dissolution operates in acidic desmutting bath, as shown by Toh et al. [18]. In this study, this severe chemical attack in the degreasing bath was consistent with the pH of the degreasing solution ($\text{pH} = 9$) and the relative instability of aluminium oxide at this pH. After pre-treatment, all the alloy surfaces showed similar scalloped morphology concerning the

shape of the pattern with slightly smaller pattern size for the polished samples.

3.1.2. Evolution of the alloy microstructure as a function of the pre-treatment steps

Table 3 reports the surface area covered by IMCs (only particles with diameter larger than $2\text{ }\mu\text{m}$ were studied) and holes for the different surfaces. Values were obtained by means of an image analysis software ImageJ with an analysis performed for a surface larger than 1 mm^2 . Before the pre-treatments, polished samples exhibited a higher surface area of IMC than laminated samples. This difference was exacerbated after degreasing, the IMC surface area on laminated sample A decreasing while it increased for polished surfaces. After the desmutting step, the IMC surface area decreased widely for all the samples and only 0.1 to 0.4% of the surface was covered by IMCs (Fig. 1c, f and i). At the same time, the surface area covered by holes, observed as black points in SEM-FEG micrographs, surged due to the IMC removal in relation with the dissolution of the matrix surrounding these particles.

EDS analyses allowed the nature of the IMCs present at the sample surfaces to be determined; the results are summarized in Fig. 3. For these analyses, more than one hundred IMCs were analysed for each sample in order to present representative results. As expected, Al-Cu-Mn-Fe (white circle in Fig. 2), Al-Cu-Mg (white square in Fig. 2) and Al-Cu (white square in Fig. 2) IMCs were identified but their distribution was very different from one sample to another one. Before the pre-treatments, alloy A presented significant differences in microstructure between the laminated and the polished samples, laminated samples showing a larger part of Al-Cu-Mn-Fe-Si particles ($> 90\%$) compared to polished samples (only 60%). A very large ratio of Al-Cu-Mg particles ($> 70\%$) was observed for polished samples of alloy B. The highest amount of Fe-rich intermetallics in alloy A could be explained by the highest Fe content of this alloy compared to alloy B, in agreement with literature data [27–31]. After degreasing, the microstructure of all samples evolved due to the IMC reactivity. As expected, for laminated samples of alloy A, no strong evolution of the microstructure was observed because the major part of the IMC was Al-Cu-Mn-Fe-Si particles, i.e. the less reactive intermetallics [25]. However, the surface area covered by these particles decreased (Table 3) which could be related to an enhanced dissolution of the matrix around these IMCs, those particles acting as cathodic sites which led to their removal. On the contrary, for polished samples of alloys A and B, the ratios of Al-Cu-Mg and Al-Cu particles significantly evolved. Again, the removal of Al-Cu-Mn-Fe particles, due to the dissolution of the surrounding matrix, could contribute to explain the evolution of the Al-Cu-Mg particle ratio. Then, the dissolution of the matrix, due to the pH value, could also explain that more IMCs could be exposed to the electrolyte after degreasing (Table 3). Moreover, the reactivity of the Al-Cu-Mg particles themselves had to be considered. These particles are known to be very reactive [32–34]. They are first anodic to the aluminium matrix and are associated to selective dissolution phenomena leading to a copper enrichment and then to an inversion of the polarity matrix/particles: the particles become cathodic to the matrix [35]. In near-neutral aqueous solutions, the dominant cathodic reaction on the copper-enriched IMCs is the oxygen reduction reaction that leads to local pH increase and promotes the dissolution of the Al matrix, causing localized attack near the IMCs and then their removal. The differences observed in the microstructure evolution between polished samples of alloys A and B could be explained considering that, even for one type of IMC, a large discrepancy could be observed in the kinetics of the reactions occurring at their surface [36]. Finally, a large number of Al-Cu-Mg particles was still present after degreasing. After desmutting, almost all IMCs were removed. The low number of residual IMCs did not allow a representative microstructure to be defined.

The results thus showed that, depending on the surface state (polished or laminated) and depending on the alloy batch, the nature of the IMCs present on the surface was significantly different before the pre-

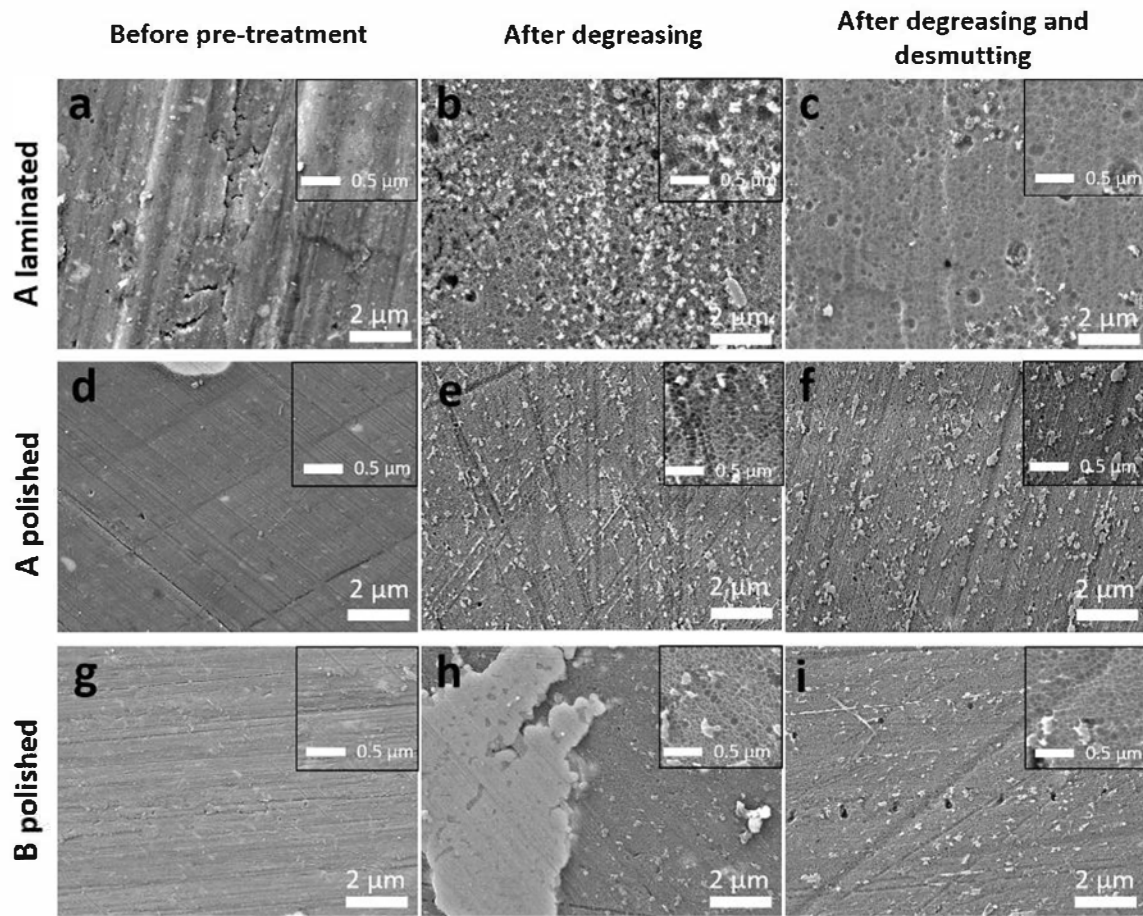


Fig. 1. SEM-FEG observations of A laminated (a, b, c), A polished (d, e, f) and B polished (g, h, i) surfaces washed with acetone (a, d, g), degreased (b, e, h) and degreased and desmutted (c, f, i).

treatments and, consequently, due to the IMC reactivity, after the pre-treatments steps. The evolution of the microstructure of the different surfaces after the degreasing and desmutting steps clearly showed the reactivity of both the IMCs and surrounding matrix. These phenomena are well-known to be associated with copper coverage of the sample surface. The IMC dealloying and dissolution/back-plating mechanism related to mechanical disconnection of Cu particles from dealloyed porous Al-Cu-Mg particles [37,38] both contribute to the copper redistribution process. However, copper redistribution could also occur from the solid solution, and in particular from the dissolution of the matrix surrounding the IMCs. Therefore, all the electrochemical processes that had occurred during the pre-treatment should lead to significant evolution of the surface reactivity. To go further in these

investigations, polarisation curves were plotted before and after the pre-treatments and the amount of electroactive copper on the sample surfaces was determined.

3.1.3. Reactivity of the sample surface and corrosion behaviour of the IMCs during the pre-treatments

Previous works showed that the reactivity of the IMCs could be studied by anodic polarisation in sodium sulphate solution [23,39]. Fig. 4 thus showed the anodic polarisation curves plotted in 0.1 M sodium sulphate for the different samples at each step of the pre-treatment. The curves plotted for the samples before the pre-treatments are also given. All curves presented a well-defined passivity plateau in good agreement with the low aggressivity of the sulphate solutions towards

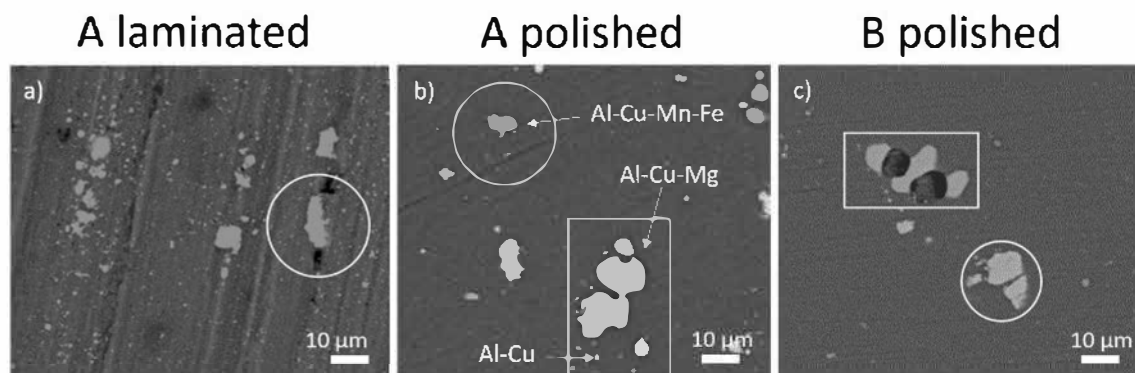


Fig. 2. SEM-FEG observations of IMCs for a) A laminated b) A polished c) B polished samples. Al-Cu-Mn-Fe IMCs are identified by means of a white circle while both Al-Cu-Mg and Al-Cu IMCs are identified with a white square.

Table 3

Surface area fractions calculated for IMCs (diameter larger than 2 μm) and holes before pre-treatments and after each pre-treatment step, for alloy A (laminated and polished samples) and alloy B (polished samples).

%	IMCs (diameter > 2 μm)			Holes		
	Before pre-treatments	After degreasing	After degreasing and desmutting	Before pre-treatments	After degreasing	After degreasing and desmutting
A laminated	0.8	0.6	0.10	0.3	0.5	0.8
A polished	1.6	2.5	0.18	0.1	0.2	0.4
B polished	1.2	2.9	0.39	0.1	0.5	1.3

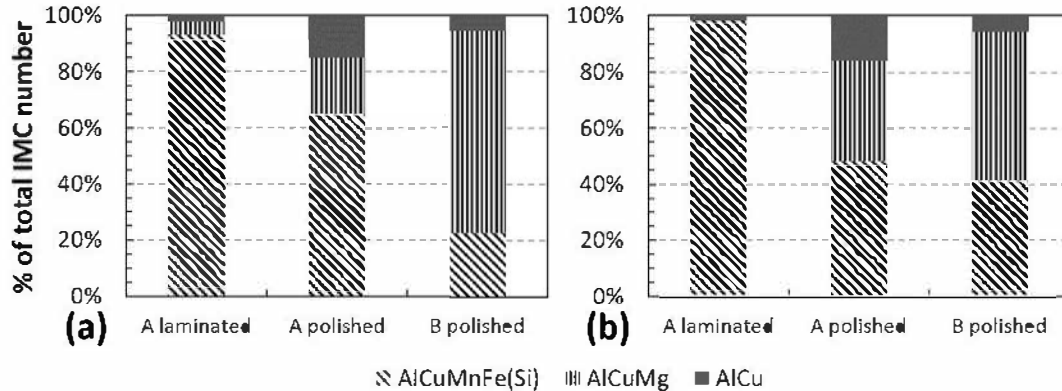


Fig. 3. Identification of the IMCs present at the surface of the samples for alloys A and B (diameter of the IMCs larger than 2 μm) before the pre-treatments (a) and after the degreasing step (b).

aluminium alloys. However, for some curves, an anodic peak (shown by an arrow) was observed between - 0.1 and 0.2 V_{SCE} that was attributed to the anodic reactions associated to the dissolution of the IMCs and subsequent surface copper coverage: the anodic peak could be attributed to the oxidation of redistributed Cu to CuO [23,39] or to the oxidation of Cu-containing IMCs [25,26]. Before the pre-treatments, only the polished samples of alloy B exhibited the characteristic peak of IMC reactivity which could be related to the large amount of Al-Cu-Mg particles in the polished surface of alloy B (Fig. 3a). After degreasing, the characteristic peak of IMC reactivity was still observed for polished samples of alloy B, in good agreement with the amount of Al-Cu-Mg particles (Fig. 3b and Table 3); this peak was also observed for laminated samples of alloy A which was more surprising considering the nature of the IMCs for these samples (Fig. 3b). This could suggest that the degreasing step modified the reactivity of Al-Cu-Mn-Fe particles. This was in good agreement with other studies that showed that a copper enrichment could be observed also for this type of IMC even if they were less reactive than Al-Cu-Mg particles [23,40]. It was also consistent with Sieradzki's results that showed that surface copper coverage could be also related to the dissolution of the solid solution surrounding the IMCs [37,38].

After the desmutting step, results clearly showed that none of the samples presented such a peak which was consistent with the important decrease of the surface area covered by the IMCs in relation with their removal (Fig. 1 and Table 3).

Therefore, the results showed differences in the reactivity of the different surfaces obtained after each step of the pre-treatment in relation with the microstructure of the samples, i.e. the nature of the IMCs present on the surface before the pre-treatments and the evolution of their distribution due to their reactivity in the pre-treatment baths. Considering that (i) the IMC dissolution can lead to copper redistribution (ii) incomplete dissolution of the IMC can leave significant localized quantities of copper [16,18,41] and (iii) copper can have a significant impact on the conversion process [42–44], the amount of electroactive copper remaining on the surface was a major parameter considering the surface properties; it was determined by CV experiments for all the samples.

3.1.4. Evolution of the electroactive copper content during the pre-treatment

The electroactive copper content was calculated from CV experiments by considering the area of the oxidation peak Cu (0) to Cu (I) with a reference value measured for pure copper at 100 a.u. as detailed by Scully and co-workers [25,26]. These authors showed that this method can be used to assay surface Cu coverage fixed by the pre-treatments. All Cu oxidation can be attributed to either surface Cu deposited on the alloy surface or Cu-containing IMCs. They also showed that the IMCs alone were a negligible source of Cu peaks in CV experiments when minimal Cu replating existed; this was especially true for pre-treated samples due to the severe IMCs removal during the pre-treatments. The relative electroactive copper content at the surface of the alloy after each step of the pre-treatment is presented in Fig. 5 for the three samples. Before pre-treatment, the electroactive copper content at the sample surface was nearly equal to zero for all the samples whereas significant amounts of electroactive copper were detected for all the samples after degreasing. Results clearly showed a large discrepancy in the copper content values measured after degreasing for all the samples. However, the increase of the electroactive copper content for laminated samples of alloy A was in good agreement with the appearance of an anodic peak on the polarisation curves (Fig. 4; the peaks are shown by the arrows) for these samples; as suggested before, the result could be explained considering a modification of the reactivity of Al-Cu-Mn-Fe particles after the exposure to the degreasing bath. For polished samples of alloys A and B, the increase of the electroactive copper content could be related to the reactivity of Al-Cu-Mg particles associated with copper redistribution, the larger amount of copper for alloy B being relevant with the presence of a peak on the polarisation curve (Fig. 4) and an higher amount of Al-Cu-Mg particles compared to alloy A. The desmutting step induced an overall decrease of the electroactive copper content in good agreement with the IMC removal and suggesting also the dissolution of the copper deposits. A significant amount of copper was still present after desmutting for the polished samples whereas no copper was detected for the laminated samples of alloy A. Such an observation confirmed that both the IMCs and the copper deposits contributed to the electroactive copper content values as proposed by Scully et al. [25,26]. For laminated samples, the

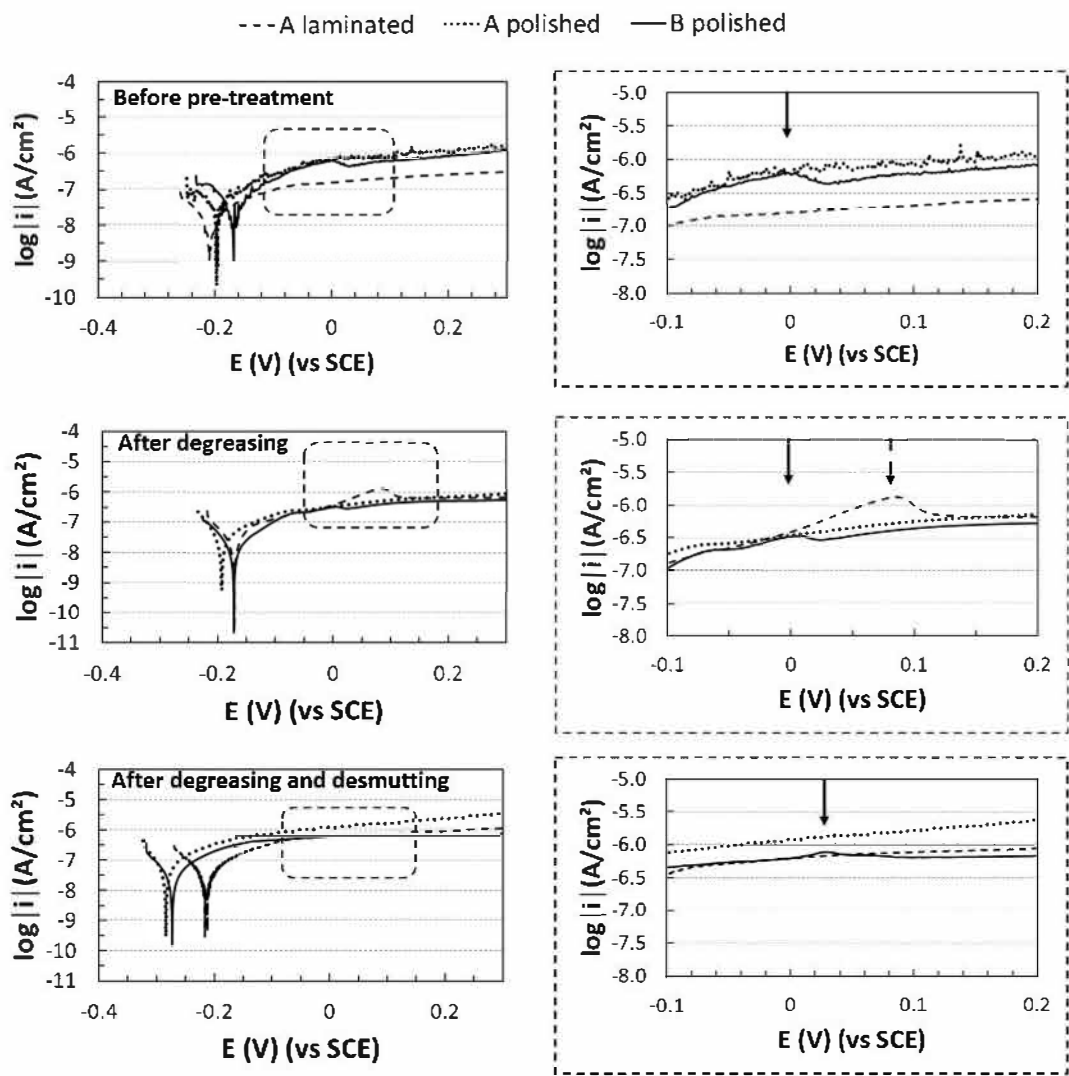


Fig. 4. Anodic polarisation curves plotted in 0.1 M Na₂SO₄ before and after each step of the pre-treatment for alloys A (polished and laminated samples) and B (polished samples). The arrows allow the anodic peak associated to the reactivity of IMCs to be identified.

electroactive copper content values measured after degreasing were mainly explained considering the activation of Al-Cu-Mn-Fe particles due to the exposure to the degreasing bath; after the desmutting step, these particles were removed leading to a copper content equal to zero. For polished samples, the electroactive copper content was explained considering both the Al-Cu-Mg particles themselves and the copper deposits so that, when the IMCs were removed after the desmutting step, the copper content was not equal to zero due to the remaining of copper deposits. Clearly, the size of the IMCs could also contribute to explain the results.

3.1.5. Wettability of the pre-treated surfaces

To complete the characterisation of the surfaces generated by the different steps of the pre-treatments, their wettability was measured. The water contact angles of the surfaces before pre-treatment and after each step of pre-treatment are given in Fig. 6. For all samples, before pre-treatment, the water contact angle was high related to the probable presence of grease and oil left by the rolling and polishing processes. The differences in water contact angle for polished and laminated samples of alloy A could be related to differences in roughness (Fig. 1). However, comparison of the results obtained after degreasing and then degreasing and desmutting for these two samples showed that the pre-

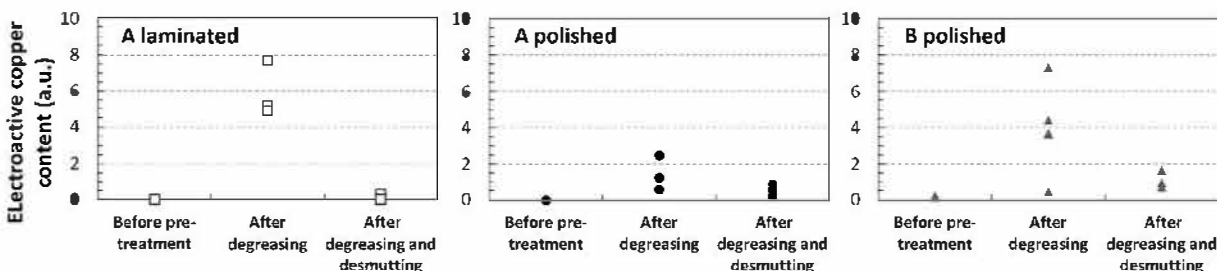


Fig. 5. Relative amount of electroactive copper content at the surface of alloys A (laminated and polished samples) and B (polished samples) before and after each step of the pre-treatment.

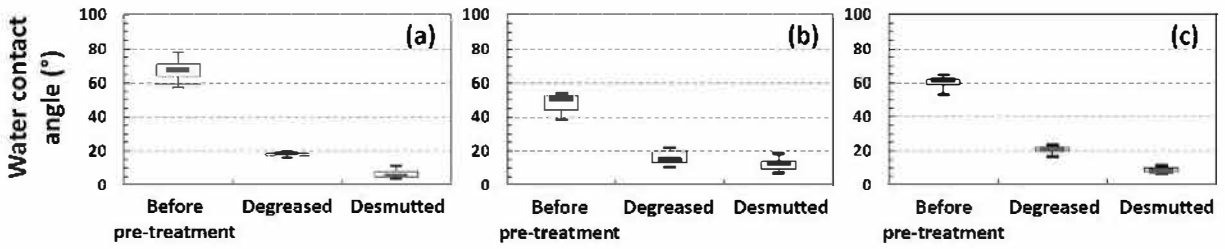


Fig. 6. Water contact angle measured before and after each step of the pre-treatment for a) laminated sample of alloy A; b) polished sample of alloy A and c) polished sample of alloy B.

treatment erased, at least partially, the influence of the initial roughness. Consequently, results obtained for the three samples after each step of the pre-treatment could be compared. After degreasing, all samples showed a lower contact angle and thus a higher wettability. At the end of the pre-treatment, all samples showed similar wettability. This led us to assume that, even if some differences in roughness still existed between the three samples at the end of the pre-treatment, they were not strong enough to modify the access of the electrolyte to the surface during the TCP coating growth. Therefore, any differences observed in the kinetics of the coating growth should not be explained totally by considering differences in roughness only.

To sum up, previous results showed that, for a same alloy, depending on its surface state (polished or laminated) and depending on its microstructure (batches A and B) before the pre-treatment, a same pre-treatment process could lead to surfaces before the conversion process which were not exactly the same. A slight difference was observed in the relative electroactive copper content between the three types of samples studied with a higher content for the polished samples and especially for alloy B. Moreover, even if, after surface treatments, the surface morphology at the microscale corresponded to a scalloped surface for all the samples, at the macroscale more defects were observed on the laminated surfaces related to the rolling process. It was now of interest to determine whether these differences could have a significant impact on the chemical conversion process and therefore modify the protective properties of the TCP coatings. To go further in this investigation, the kinetics of growth, structure, morphology and protective properties of the TCP coatings were studied.

3.2. Characterisation and properties of the TCP coatings

3.2.1. Kinetics of growth of the TCP coatings

The OCPs of the three samples after pre-treatment during immersion in the conversion solution (Socosurf TCS) are shown in Fig. 7. Globally, the shape of the curves was the same for all samples: the OCP displayed an initial rapid fall, a subsequent small peak and a gradual rise to a relatively steady state value. According to literature [9,16,45,46], the initial decrease of the OCP was attributed to thinning of the air-formed oxide film on the alloy surface. Such a thinning enabled the electrochemical reactions to proceed [47]. Then, the OCP increase was related

to the deposition of the conversion layer on the alloy surface. The OCP plateau observed should be correlated to a complete coverage of the alloy surface by the TCP coating. As suggested by Andreatta et al. [46], further deposition on the alloy surface should lead to an increase of the thickness of the conversion layer without affecting the OCP. Comparison of the three curves showed that the minimal OCP value was less negative (-1.02 V/SCE) for polished sample of alloy B compared to laminated sample (-1.05 V/SCE) and polished sample (-1.10 V/SCE) of alloy A. Further, considering that the OCP was stable when the difference between two successive values was < 0.003 V (blue lines in Fig. 7), the OCP curves suggested that the surface of the samples was completely covered by the TCP coating after about 32 s, 33 s and 37 s for laminated sample of alloy A, polished sample of alloy B and polished sample of alloy A respectively. Therefore the growth of the TCP coating was assumed to be slightly faster on laminated sample of alloy A and polished sample of alloy B compared to polished sample of alloy A. The difference in the kinetics of growth of the TCP coatings should be linked to the roughness but also to differences in chemistry of the surface after the pre-treatment. According to literature, the mechanism of deposition was based on the local raise of pH on the alloy surface. During the OCP decrease, the initial oxide film is dissolved due to fluoride ions leading to the dissolution of aluminium and a shift of the electrode potential to the negative direction. Protons and oxygen reduction occurs accompanied by a local increase in pH which favors the precipitation of hydrated zirconia film and hydrated chromium oxide [7]. Li et al. [17] showed that, with a greater surface roughness, the TCP coating formed less completely leading to a less-continuous coating which was in agreement with our results. Therefore, even if differences in water contact angle were not significant for the different surfaces after pre-treatment (Fig. 6), the greater roughness observed for laminated sample of alloy A increased slightly the kinetics of growth of the TCP coating. Moreover, previous results showed that at least the initial stages of coating growth could be affected by electroactive copper before it is covered by the growing coating [9,16,45]. Indeed, electroactive copper constitutes cathodic sites where protons and oxygen reduction can occur leading to a local increase of pH that promotes the precipitation of chromium- and zirconium-rich layer. The stronger surface copper coverage observed for polished sample of alloy B should explain a fast kinetics of growth of the TCP coating.

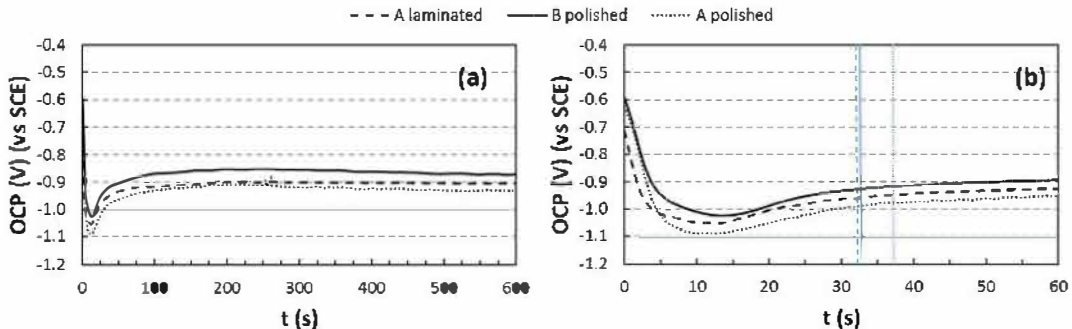


Fig. 7. a) Variation of the OCP of the pre-treated AA 2024 - T3 with immersion time in the conversion bath (Socosurf TCS). Curves are plotted for polished samples of alloys A and B and laminated sample of alloy A. b) Zoom on the first times of the coating growth.

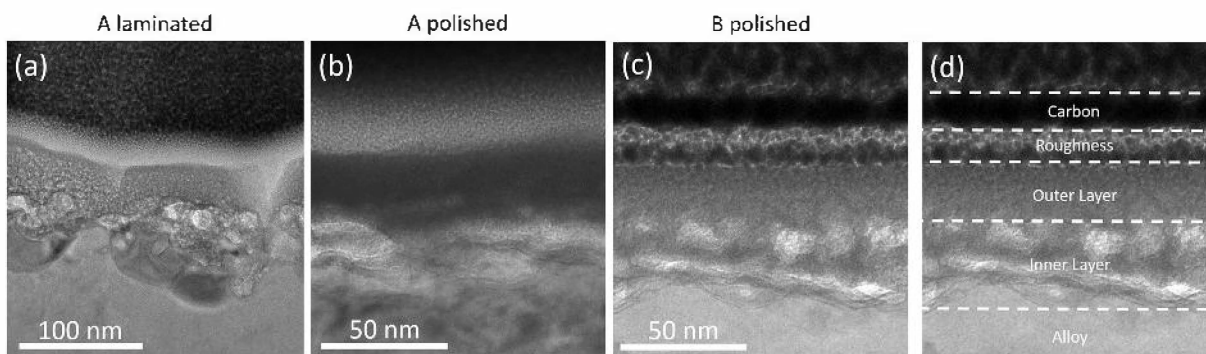


Fig. 8. TEM images of the cross-sections of the TCP coatings grown on AA 2024 - T3 samples for a) laminated sample of alloy A, b) polished sample of alloy A and c) polished sample of alloy B. The different layers are clearly indicated in figure d) (corresponding to image c). TEM observations are performed for TCP coatings without the post-treatment in PACS bath.

3.2.2. Structure and morphology of the TCP coatings

TEM images of the cross-sections of the TCP coatings grown during immersion of the AA 2024 samples in the conversion bath without the PACS post-treatment are shown in Fig. 8. Independent of the samples, the TCP coating was formed of two distinct layers. EDS line analysis allowed to distinguish an outer layer mainly composed of chromium and zirconium oxide, hydroxide and/or oxy-hydroxide and an inner part corresponding to a mixture of aluminium fluoride and aluminium oxide as previously shown by different authors [7,48]. Another important aspect was the difference in thickness between the different samples assessed by different TEM observations. For polished sample of alloy A, the total thickness of the layer was around 50 nm (Fig. 8 b). For polished sample of alloy B (Fig. 8 c), the total thickness could be evaluated between 60 and 75 nm taking into account or not an external defective layer called as “roughness” in Fig. 8 d. For the laminated sample of alloy A, a strong heterogeneity in thickness of the TCP coating was observed (Fig. 8 a) with 50 nm thick zones comprised between zones with a thickness of about 115 nm. TEM observations were well-correlated with the kinetics of growth of the TCP coatings (Fig. 7). Indeed, a fast growth of the TCP coating on the sample surface could lead to the formation of a thicker coating as shown by Viroulaud et al. [48] by means of ToF-SIMS analyses. These authors also showed that a quick growth was associated with a less homogeneous TCP coating which was observed, considering the thickness, for polished sample of alloy B and even more for laminated sample of alloy A. To complete the results, representative SEM-FEG observations of the surface of the TCP coated samples after the post-treatment in the PACS bath were performed (Fig. 9). Observations clearly showed a low surface roughness with some growth defects for the polished samples. On the contrary, after the conversion process, the laminated samples of alloy A showed large growth defects at the surface and some cracks. The cracks could be related to the stresses generated by differences in the kinetics of coating growth above different zones of the surface but it could also be due to the exposure to vacuum in the SEM.

3.2.3. Study of the coating protective properties in sulphate solutions

First, the protective properties of the TCP coatings after PACS post treatment were determined in a low-aggressive solution, i.e. a 0.1 M Na_2SO_4 solution by means of EIS analysis. EIS measurements were performed for all coated alloys for immersion times varying from 0 to 28 days. As an example, Fig. 10 presents the EIS spectra plotted for the TCP coated samples after two different immersion times (0 and 14 days) at the OCP in naturally aerated 0.1 M Na_2SO_4 solution. Independent of the immersion time, all the samples showed similar EIS spectra. Visual evaluation of the spectra would lead to the identification of one time constant; however, the analysis using equivalent circuits showed that the difference between the fitted and the experimental data was the lowest using the equivalent circuit proposed by Qi et al. (Fig. 11) based on the identification of two time constants, likely related to the conversion coating itself and the electrochemical processes occurring at the coating/alloy interface [9]. This circuit comprises the electrolyte resistance (R_e), a parallel combination of the charge transfer resistance R_{ct} and a constant phase element Q_{dl} , and finally the coating resistance R_{coat} associated with another constant phase element Q_{coat} . Visual inspection of the EIS spectra showed that, at the beginning of the immersion ($t = 0$ day), the impedance modulus at $5 \cdot 10^{-2}$ Hz ($|Z|_{0.05\text{Hz}}$) measured for 3 different surfaces can be ranked: polished alloy A > polished alloy B > laminated alloy A. As already shown by other authors [49], higher impedance modulus is associated with improved corrosion protection of the coating which could be related to a less defective coating or to better adhesion of the coating on the metal. Moreover, the frequency ranges where high phase angles ($< -70^\circ$; within grey zone in Fig. 10) appeared were $5 \cdot 10^{-2}$ – $3 \cdot 10^1$ Hz for laminated alloy A, $\approx 3 \cdot 10^{-3}$ – $5 \cdot 10^1$ Hz for polished alloy A and $1 \cdot 10^{-2}$ – $5 \cdot 10^1$ Hz for polished alloy B. The measured frequency range of high phase angles can be narrower with increasing coating capacitance and suggested reduced corrosion protection of the coating as shown by other authors [9,49,50]. This could be related to easier penetration of the electrolyte through defects of the coating. The results thus showed that both the TCP coatings grown on laminated sample of alloy A and

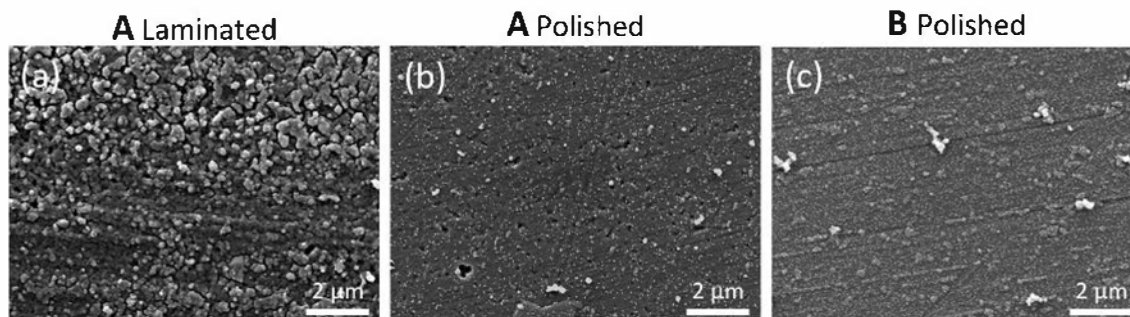


Fig. 9. SEM-FEG observations of the TCP coated samples with the PACS post-treatment for a) laminated sample of alloy A b) polished sample of alloy A and c) polished sample of alloy B.

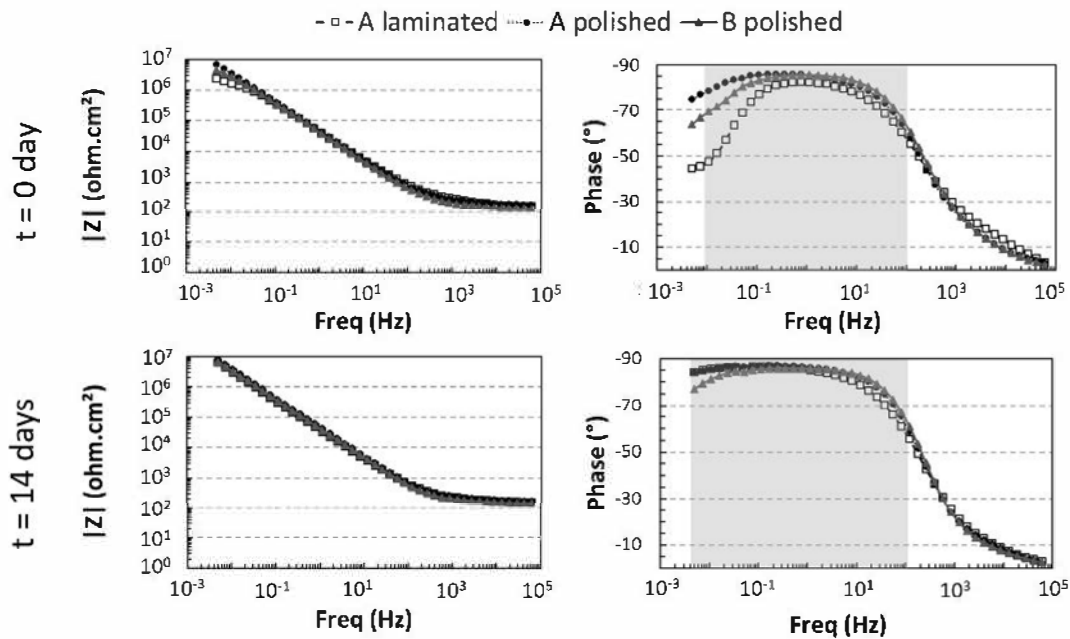


Fig. 10. EIS spectra plotted for TCP coated samples with the PACS post-treatment (polished and laminated samples of alloy A and polished sample of alloy B) after 0 day (top) and 14 days (down) of immersion in naturally aerated 0.1 M Na_2SO_4 at OCP.

polished sample of alloy B had lower protective properties than that grown on polished sample of alloy A. This could be explained by referring to previous results. First, for laminated samples of alloy A, the defects observed by SEM-FEG (Fig. 9) should explain the lower protective properties of the TCP coating grown on this alloy. This was in agreement with works of Li et al. [17] who showed that the TCP coating formed less completely and with more defects on a surface with greater surface roughness. Concerning the polished sample of alloy B, the surface copper coverage measured after the pre-treatment should contribute to explain the results. However, this was not consistent with the work of Qi et al. [16] who showed that a pre-treatment that left copper-rich sponges led to more protective coatings. Further, Viroulaud et al. [48] concluded from their work that the presence of copper was not the main parameter. As suggested by these authors, a key parameter could be the kinetics of coating growth: a fast kinetics would lead to a thicker TCP coating with some heterogeneities and thus more susceptible to cracking. This hypothesis was consistent with our results; indeed, both laminated sample of alloy A and polished sample of alloy B showed a faster kinetics of coating growth associated with a thicker TCP coating. However, another point of interest was the EIS measurements performed after 14 days of immersion: for these conditions, no significant difference was observed between all the coated samples, except that the measured frequency range of high phase angles was a little narrower

(within grey zone in Fig. 10) for polished sample of alloy B. This suggested that a self-healing mechanism could contribute to repair the defects present inside the TCP coating.

In order to evaluate more properly the protective properties of the coating, an attempt was made to determine the parameters of the previously described equivalent circuit (Fig. 11). The values calculated for 0 and 14 days of immersion are summarized in Table 4 in order to give quantitative data while Fig. 12 enables to show the evolution of the parameters as a function of the immersion time for the whole duration of the experiments (28 days). However, these values had to be considered with precautions because the differences between the experimental results and fitted data remained significant which was probably due to the heterogeneity of the TCP coatings.

Nevertheless, some comments deserved to be done. First, it was of interest to note that, for all the coated samples, independent of the immersion time, R_{coat} values were of the order of the electrolyte resistance which indicated a high permeability allowing access of the electrolyte to the alloy through pores and cracks. This suggested once more that the TCP coatings presented some heterogeneities. On the contrary, R_{ct} values were much higher (in the range of $10^8 \Omega \cdot \text{cm}^2$) showing that the protective properties of the coating were mainly due to its inner layer [9]. Globally, all the resistance values were in the same range of order when the three samples were compared. However,

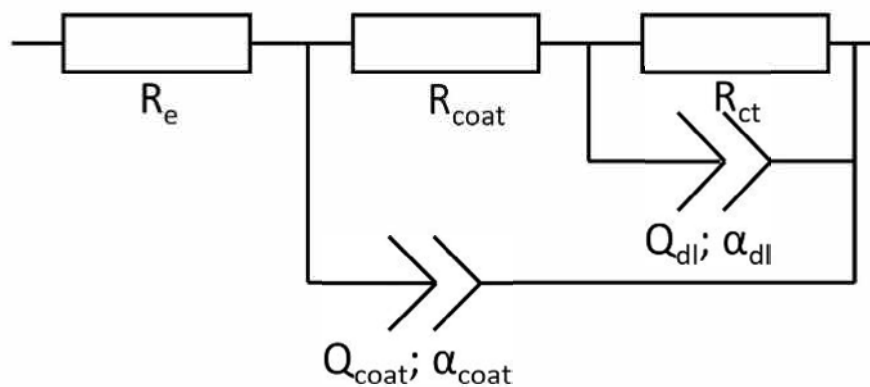


Fig. 11. Equivalent circuit used to fit the EIS spectra plotted for the TCP coated samples with the PACS post-treatment [9].

Table 4Parameters extracted from EIS spectra using the equivalent circuit of Fig. 11 for TCP coated samples exposed to a 0.1 M Na₂SO₄ solution at OCP.

Alloy	Surface state	Immersion time (day)	R _{ct}	R _{coat}	Q _{dl}	Q _{coat}	α _{dl}	α _{coat}
			Ω·cm ²		10 ⁻⁶ s ⁿ /(Ω·cm ²)			
A	Laminated	0	3.30·10 ⁶	346	2.4	1.9	0.92	0.86
		14	237·10 ⁶	318	2.8	1.8	0.95	0.95
	Polished	0	37.0·10 ⁶	271	2.3	1.2	0.94	0.94
		14	295·10 ⁶	178	2.5	1.1	0.96	0.96
B	Polished	0	11.0·10 ⁶	149	3.3	0.87	0.92	1
		14	42.9·10 ⁶	105	3.2	0.89	0.94	1

one of the main results was probably that B polished sample exhibited the lowest R_{ct} and R_{coat} values, for all the immersion times (except 0 day for R_{ct} values), indicating the lowest protective properties of the coating developed on its surface. This was in agreement with previous explanations. The low R_{coat} values, despite of a thick TCP coating, suggested the presence of a large number of defects such as cracks. As previously said, these cracks were most probably due to differences in kinetics of coating growth over the whole surface of the pre-treated alloy in relation with the presence of copper deposits. Concerning the laminated sample of alloy A, the low R_{ct} values measured for this sample, in particular at the very first stage of immersion, confirmed the low protective properties of the TCP coating in agreement with previous explanations. However, this sample showed also the highest R_{coat} values. This could be explained by referring to Qi's work [9] who showed that, by increasing the time of the coating treatment for a pure aluminium sample, R_{ct} values decreased while R_{coat} values increased. The author attributed the decrease of R_{ct} to the accumulations of fluoride ions at the base of the coating and the increase of R_{coat} to a combination of an increase of the coating thickness and change in the coating morphology. Our previous results (Figs. 7 and 8) showed that the TCP coating grown on laminated sample of alloy A was the thickest which was in good agreement with the high R_{coat} values. Further, the

great initial roughness should explain the accumulation of fluoride ions near the base of the coating, at least on some parts of the surface, reducing the protective properties of this coating as suggested also by Viroulaud et al. [48]. Concerning the CPE parameters, as previously said, values had to be considered with precautions but the lower α_{coat} combined with higher Q_{coat} values at the beginning of the immersion for laminated sample of alloy A compared to other samples suggested a strong heterogeneity of the coating in agreement with previous comments. Moreover, results confirmed a lower corrosion protection at the beginning of the immersion for laminated sample of alloy A and polished sample of alloy B with an enlarged Q_{dl} and smaller exponent n_{dl} [49,51]. Finally, results showed that all parameters only slightly evolved as a function of the immersion time which could be related to the low aggressivity of the electrolyte.

Therefore, the results showed that, depending on the microstructure and surface state of the alloy before the pre-treatment, the properties of the surface obtained after the pre-treatment step could be different leading to measurable differences in the protective performance of the TCP coatings in low-aggressive solution.

3.2.4. Study of the coating protective properties in chloride solutions

To complete the results, OCP measurements and potentiodynamic

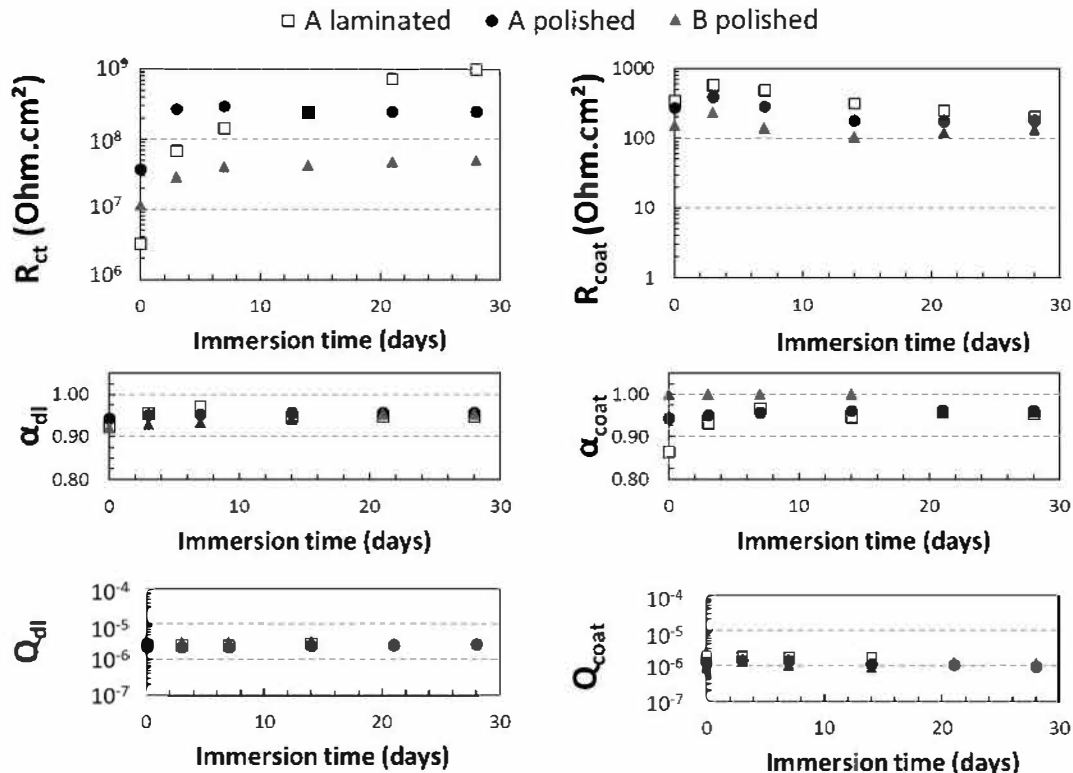


Fig. 12. Parameters for the TCP coated samples with the PACS post-treatment (polished and laminated samples of alloy A and polished sample of alloy B) vs the immersion time in naturally aerated 0.1 M Na₂SO₄ solution. Parameters are extracted from EIS data using the equivalent circuit given in Fig. 11.

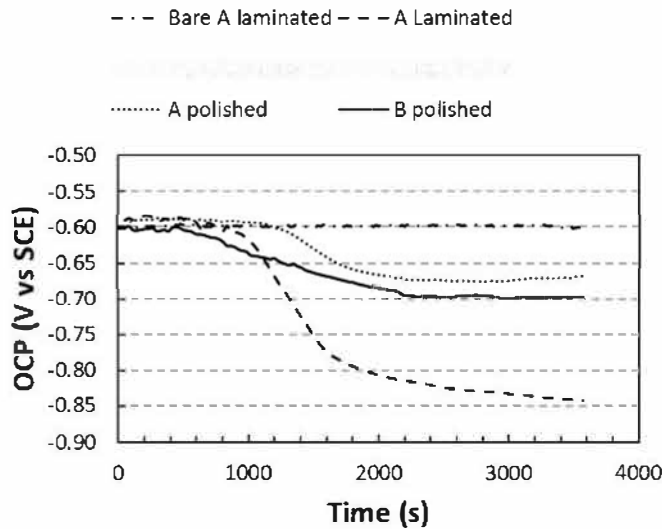


Fig. 13. OCP versus immersion time in 0.5 M NaCl solution for the TCP coated samples with the PACS post-treatment (polished and laminated samples of alloy A and polished sample of alloy B). The OCP curve was also reported for the bare laminated sample of alloy A for comparison.

polarisations were performed in 0.5 M NaCl solution. NaCl solution was assumed to be more representative of the in-service conditions; furthermore, it was also more representative of the industrial tests such as neutral salt spray tests. Fig. 13 shows the OCP versus immersion time in 0.5 M NaCl conditions for the TCP coated samples after PACS post-treatment. All curves showed relatively stable OCP values in the first 10 min (600 s in Fig. 13); the values were similar for the three samples. Then, the OCP values decreased to reach after 40 min (2400 s) a plateau value of -0.67 V vs SCE and -0.70 V vs SCE for polished sample of alloy A and B respectively. The experiments were performed at least three times and the results were reproducible for the two samples. For laminated sample of alloy A, the OCP curves exhibited a stronger decrease after 10 min and reached after about 1 h a plateau with OCP values comprised between of -0.85 V vs SCE and -0.73 V vs SCE. This lack of reproducibility in the OCP plateau values for the laminated sample of alloy A should be related to the heterogeneities observed in the TCP coating (Figs. 8 and 9) which could vary from one sample to another. In the same solution, the bare alloys showed stable OCP values at around -0.6 V vs SCE. For the three TCP coated samples, the more negative OCP values reached after 1 h of immersion compared to the bare alloy should be related to a reduction of the kinetics of the oxygen reduction on the sample surface due to the TCP coating [7]. The existence of two OCP plateaus suggested that the TCP coatings evolved during immersion in the electrolyte as previously observed in sulphate solution (Fig. 10) with a slight increase of $|Z|_{0.05\text{Hz}}$ between 0 and 14 days of immersion. All results were also in agreement with potentiodynamic results (Table 5). Comparison of the potentiodynamic polarisation curves in the cathodic domain showed that the cathodic current densities were shifted towards lower values for the TCP coated samples compared to the bare samples. For the bare samples, the values

Table 5
Values deduced from the potentiodynamic polarisation curves plotted after 1 h at the OCP. All experiments were performed in 0.5 M NaCl solution for the TCP coated samples (polished and laminated samples of alloy A and polished sample of alloy B).

Samples	i_{cath} (A cm^{-2}) at $E = -0.9$ V vs SCE	E_{corr} (V vs SCE)	i_{corr} (A cm^{-2})	E_{pit} (V vs SCE)
Bare laminated A	$4 \cdot 10^{-5}$	-0.59	$3 \cdot 10^{-6}$	-0.59
TCP coated samples				
Laminated A	$1 \cdot 10^{-6}$	-0.74	$6.3 \cdot 10^{-8}$	-0.60
Polished A	$1 \cdot 10^{-6}$	-0.67	$7.9 \cdot 10^{-8}$	-0.57
Polished B	$1 \cdot 10^{-6}$	-0.70	$1 \cdot 10^{-8}$	-0.59

are given for the laminated sample of alloy A only; similar values are obtained for the other bare alloys. This confirmed that the TCP coatings reduced the oxygen availability near the substrate, resulting in cathodic inhibition [16,52]. Furthermore, when the curves were plotted after only 10 min of immersion in the chloride solution (results not shown), only a very short passivity plateau was observed while the passivity plateau was larger when the curves were plotted after 1 h of immersion. This suggested once more either a modification of the TCP coating thickness or a change in the structure, at least in the external layer, during immersion in the electrolyte. Another important result was that, for all coated samples, pitting was observed with similar values of E_{pit} for all samples. The results therefore showed that the TCP coatings provided an efficient protection against corrosion mainly due to physical blocking by the TCP coating of the oxygen reduction. However, no significant differences were observed between the three coated samples with similar cathodic current densities and E_{pit} values. EIS measurements (not shown) led to the same conclusions. This suggested that the differences in protective properties measured previously in a low-aggressive solution were not significant in a more aggressive solution.

3.2.5. Comparison with industrial tests

Because the protective properties of conversion coatings are of major importance for the aeronautical industry, we chose to test also the coating performance using industrial tests, i.e. neutral salt spray tests (NSS). NSS results, reported in Fig. 14, showed that all the coated samples exhibited at least one pit after 300 h of exposure and > 5 pits after 450 h. This was consistent with previous results that showed only slight differences in protective performance between the different samples in a low-aggressive solution and no significant differences in NaCl solution. This highlighted also that NSS were too much aggressive to distinguish between different conversion coatings while even slight differences in protective properties could be shown in low aggressive solution.

4. Conclusions

The protective properties of TCP coatings grown on alloy 2024-T3 were studied for two different batches; the influence of the initial surface state (laminated and polished) was studied also. The main conclusions are the following.

- 1) In a low-aggressive solution, i.e. 0.1 M Na_2SO_4 , the protective properties of the TCP coatings decreased when the roughness of the initial surface increased. Furthermore, improved protective

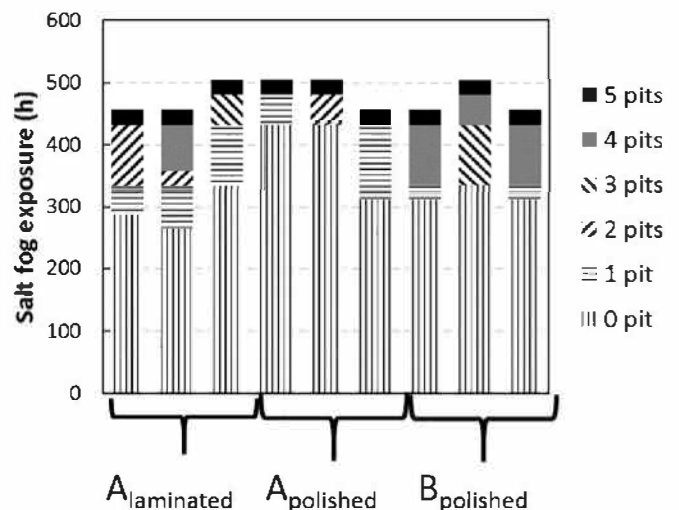


Fig. 14. Neutral salt spray test results obtained for TCP coated samples with the PACS post treatment of alloys A and B.

properties were observed for a TCP coating grown on a surface with a low surface copper coverage in relation with a low amount of Al-Cu-Mg IMCs in the initial microstructure.

- 2) The most plausible explanation is that a fast kinetics of coating growth, either associated to strong initial roughness or a great surface copper coverage, was detrimental for the protective properties of the coatings. This led to thicker coatings more susceptible to cracks.
- 3) In more aggressive solutions, i.e. 0.5 M NaCl solution, the differences are not significant: all measurements showed a similar decrease of the oxygen reduction, compared to bare alloy, due to the TCP coating and the same susceptibility to pitting. This was in agreement with neutral salt spray tests.
- 4) For industrial applications, the results showed that variations in batches, for a same type of alloy, or in initial surface state should not be detrimental for the corrosion resistance of the TCP coated samples. However, more significant differences in the alloy microstructure could have a greater effect on the protective properties of the TCP coatings. The conversion process has therefore to be adapted for different types of alloys.

Acknowledgements

The authors thank Mecaprotect and the ANRT for their financial support.

References

- [1] Properties and selections, ASM International, 10th edition, Materials Park, Ohio, 1990.
- [2] T. Muster, A.E. Hughes, G.E. Thompson, Copper Distribution in Al Alloys, Nova Science Publishers, 2007.
- [3] A.E. Hughes, G.E. Thompson, J.M. Mol, N. Biribilis, S.J. Garcia, X. Zhou, High Strength Al-Alloys: Microstructure, Corrosion and Principles of Protection, INTECH Open Access Publisher, 2011.
- [4] European Chemical Agency, REACH annex XIV, (2013).
- [5] L. Li, G.P. Swain, A. Howell, D. Woodbury, G.M. Swain, The formation, structure, electrochemical properties and stability of trivalent chrome process (TCP) coatings on AA2024, J. Electrochem. Soc. 158 (2011) C274–C283.
- [6] Y. Guo, A Study of Trivalent Chrome Process Coatings on Aluminum Alloy 2024-T3, The Ohio State University, 2011.
- [7] Y. Guo, G.S. Frankel, Characterization of trivalent chromium process coating on AA2024-T3, Surf. Coat. Technol. 206 (2012) 3895–3902.
- [8] C. Cai, X.-Q. Liu, X. Tan, G.-D. Li, H. Wang, J.-M. Li, J.-F. Li, A Zr- and Cr(III)-containing conversion coating on Al alloy 2024-T3 and its self-repairing behavior: conversion coating on Al alloy 2024-T3 and its self-repairing behavior, Mater. Corros. 68 (2017) 338–346.
- [9] J.-T. Qi, T. Hashimoto, J.R. Walton, X. Zhou, P. Skeldon, G.E. Thompson, Trivalent chromium conversion coating formation on aluminium, Surf. Coat. Technol. 280 (2015) 317–329.
- [10] S. Joshi, W.G. Fahrenholtz, M.J. O'Keefe, Effect of alkaline cleaning and activation on aluminum alloy 7075-T6, Appl. Surf. Sci. 257 (2011) 1859–1863.
- [11] C.E. Moffitt, D.M. Wieliczka, H.K. Yasuda, An XPS study of the elemental enrichment on aluminum alloy surfaces from chemical cleaning, Surf. Coat. Technol. 137 (2001) 188–196.
- [12] W. Pinc, S. Geng, M. O'Keefe, W. Fahrenholtz, T. O'Keefe, Effects of acid and alkaline based surface preparations on spray deposited cerium based conversion coatings on Al 2024-T3, Appl. Surf. Sci. 255 (2009) 4061–4065.
- [13] T.G. Harvey, A.E. Hughes, S.G. Hardin, T. Nikpour, S.K. Toh, A. Boag, D. McCulloch, M. Horne, Non-chromate deoxidation of AA2024-T3: sodium bromate–nitric acid (20–60 °C), Appl. Surf. Sci. 254 (2008) 3562–3575.
- [14] Y. Liu, M.A. Arenas, S.J. Garcia-Vergara, T. Hashimoto, P. Skeldon, G.E. Thompson, H. Habazaki, P. Bailey, T.C.Q. Noakes, Behaviour of copper during alkaline corrosion of Al–Cu alloys, Corros. Sci. 50 (2008) 1475–1480.
- [15] Y. Liu, M.A. Arenas, A. de Frutos, J. de Damborenea, A. Conde, P. Skeldon, G.E. Thompson, P. Bailey, T.C.Q. Noakes, Influence of nitric acid pre-treatment on Al–Cu alloys, Electrochim. Acta 53 (2008) 4454–4460.
- [16] J. Qi, A. Němcová, J.R. Walton, X. Zhou, P. Skeldon, G.E. Thompson, Influence of pre- and post-treatments on formation of a trivalent chromium conversion coating on AA2024 alloy, Thin Solid Films 616 (2016) 270–278.
- [17] L. Li, A.L. Desouza, G.M. Swain, Effect of deoxidation pretreatment on the corrosion inhibition provided by a trivalent chromium process (TCP) conversion coating on AA2024-T3, J. Electrochem. Soc. 161 (2014) C246–C253.
- [18] S.K. Toh, A.E. Hughes, D.G. McCulloch, J. du Plessis, A. Stonham, Characterization of non-Cr-based deoxidizers on Al alloy 7475-T7651, Surf. Interface Anal. 36 (2004) 1523–1532.
- [19] C.M. Rangel, T.I. Paiva, P.P. da Luz, Conversion coating growth on 2024-T3 Al alloy. The effect of pre-treatments, Surf. Coat. Technol. 202 (2008) 3396–3402.
- [20] J. Qi, T. Hashimoto, J. Walton, X. Zhou, P. Skeldon, G.E. Thompson, Formation of a trivalent chromium conversion coating on AA2024-T351 alloy, J. Electrochem. Soc. 163 (2016) C25–C35.
- [21] K. Thirupathi, P. Barczy, B.M. Somosvári, Impact of corrosive liquid on trivalent chromium over aluminium alloys, J. Surf. Eng. Mater. Adv. Technol. 07 (2017) 51–60.
- [22] A. Sarfraz, R. Posner, M.M. Lange, K. Lill, A. Erbe, Role of intermetallics and copper in the deposition of ZrO₂ conversion coatings on AA6014, J. Electrochem. Soc. 161 (2014) C509–C516.
- [23] C. Blanc, S. Gastaud, G. Mankowski, Mechanistic studies of the corrosion of 2024 aluminum alloy in nitrate solutions, J. Electrochem. Soc. 150 (2003) B396–B404.
- [24] A.J. Davenport, R.G. Bin, Copper accumulation during Cleaning of Al-Cu alloys, Corros. Corros. Prev. Low Density Met. Alloys Proc. Int. Symp. The Electrochemical Society, 2001, pp. 41–46.
- [25] M.A. Jakab, D.A. Little, J.R. Scully, Experimental and modeling studies of the oxygen reduction reaction on AA2024-T3, J. Electrochem. Soc. 152 (2005) B311–B320.
- [26] D.A. Little, M.A. Jakab, J.R. Scully, Effect of surface pretreatment on the underpaint corrosion of AA2024-T3 at various temperatures, Corrosion 62 (2006) 300–315.
- [27] L. Sweet, S.M. Zhu, S.X. Gao, J.A. Taylor, M.A. Easton, The effect of iron content on the iron-containing intermetallic phases in a cast 6060 aluminum alloy, Metall. Mater. Trans. A 42 (2011) 1737–1749.
- [28] M. Dash, M. Makhlof, Effect of key alloying elements on the feeding characteristics of aluminum-silicon casting alloys, J. Light. Met. 1 (2001) 251–265.
- [29] Y. Zhao, C.C. Wang, X. Wang, J.C. Huang, G.F. Zhang, M.T. Wang, Z.C. Zhang, M. Wu, Effects of precipitation behaviors on the microstructure and fracture toughness of Al-Cu-Mg aluminum alloys, Optoelectron. Adv. Mater. 10 (2016) 583–589.
- [30] Y. Liu, L. Luo, C. Han, L. Ou, J. Wang, C. Liu, Effect of Fe, Si and cooling rate on the formation of Fe- and Mn-rich intermetallics in Al–5Mg–0.8Mn alloy, J. Mater. Sci. Technol. 32 (2016) 305–312.
- [31] U. Patakham, C. Limmaneevichitr, Effects of iron on intermetallic compound formation in scandium modified Al–Si–Mg Alloys, J. Alloys Compd. 616 (2014) 198–207.
- [32] C. Blanc, B. Lavelle, G. Mankowski, The role of precipitates enriched with copper on the susceptibility to pitting corrosion of the 2024 aluminum alloy, Corros. Sci. 39 (1997) 495–510.
- [33] V. Guillaumin, G. Mankowski, Localized corrosion of 2024 T351 aluminium alloy in chloride media, Corros. Sci. 41 (1998) 421–438.
- [34] M. Elboujdaini, E. Ghali, An electrochemical investigation of the behaviour of aluminium alloys in different electrolytes, Corros. Sci. 30 (1990) 855–867.
- [35] R.G. Buchheit, M.A. Martinez, L.P. Montes, Evidence for Cu ion formation by dissolution and dealloying the Al₂CuMg intermetallic compound in rotating ring-disk collection experiments, J. Electrochem. Soc. 147 (2000) 119–124.
- [36] L. Lacroix, L. Ressler, C. Blanc, G. Mankowski, Statistical study of the corrosion behaviour of Al₂CuMg intermetallics in AA2024 T351 by SKPFM, J. Electrochem. Soc. 155 (2008) C8–C15.
- [37] M.B. Vukmirovic, N. Dimitrov, K. Sieradzki, Dealloying and corrosion of Al alloy 2024T3, J. Electrochem. Soc. 149 (2002) B428–B439.
- [38] N. Dimitrov, J.A. Mann, K. Sieradzki, Copper redistribution during corrosion of aluminum alloys, J. Electrochem. Soc. 146 (1999) 98–102.
- [39] P. Carbonini, T. Monetta, D.B. Mitton, F. Bellucci, P. Mastronardi, B. Scatteia, Degradation behaviour of 6013-T6, 2024-T3 alloys and pure aluminium in different aqueous media, J. Appl. Electrochem. 27 (1997) 1135–1142.
- [40] P. Schmutz, G.S. Frankel, Corrosion study of AA2024-T3 by scanning kelvin probe force microscopy and in situ atomic force microscopy scratching, J. Electrochem. Soc. 145 (1998) 2295–2306.
- [41] A.E. Hughes, G. Theodossiou, S. Elliott, T.G. Harvey, P.R. Miller, J.D. Gorman, P.J.K. Paterson, Study of deoxidation of 2024-T3 with various acids, Mater. Sci. Technol. 17 (2001) 1642–1652.
- [42] Q. Meng, G.S. Frankel, Effect of copper content on chromate conversion coating protection of 7xxx-T6 aluminum alloys, Corrosion 60 (2004) 897–905.
- [43] X. Sun, R. Li, K.C. Wong, K.A.R. Mitchell, T. Foster, Surface effects in chromate conversion coatings on 2024-T3 aluminum alloy, J. Mater. Sci. 36 (2001) 3215–3220.
- [44] J. Qi, Y. Miao, Z. Wang, Y. Li, X. Zhang, P. Skeldon, G.E. Thompson, Influence of copper on trivalent chromium conversion coating formation on aluminum, J. Electrochem. Soc. 164 (2017) C611–C617.
- [45] J. Cerezo, I. Vandendael, R. Posner, K. Lill, J.H.W. de Wit, J.M.C. Mol, H. Terryn, Initiation and growth of modified Zr-based conversion coatings on multi-metal surfaces, Surf. Coat. Technol. 236 (2013) 284–289.
- [46] F. Andreatta, A. Turco, I. de Graeve, H. Terryn, J.H.W. de Wit, L. Fedrizzi, SKPFM and SEM study of the deposition mechanism of Zr/Ti based pre-treatment on AA6016 aluminum alloy, Surf. Coat. Technol. 201 (2007) 7668–7685.
- [47] L. Fedrizzi, F. Deflorian, P.L. Bonora, Corrosion behaviour of fluotitanate pretreated and painted aluminium sheets, Electrochim. Acta 42 (1997) 969–978.
- [48] R. Viroulaud, J. Swiatowska, A. Seyeux, S. Zanna, J. Tardelli, Ph. Marcus, Influence of surface pretreatments on the quality of trivalent chromium process coatings on aluminum alloy, Appl. Surf. Sci. 423 (2017) 927–938.
- [49] J. Qi, L. Gao, Y. Li, Z. Wang, G.E. Thompson, P. Skeldon, An optimized trivalent chromium conversion coating process for AA2024-T351 alloy, J. Electrochem. Soc. 164 (2017) C390–C395.
- [50] C.A. Matzdorf, W.C. Nickerson, E. Lipnickas, Evaluation of modified zirconium/trivalent chromium conversion coatings by accelerated corrosion and electrochemical techniques, 2005 Tri-Service Corrosion Conference, Orlando, Florida, U.S.A, 2005, NACE International, Orlando, Florida, U.S.A, 2005, pp. 1–22.
- [51] J. Creus, H. Mazille, H. Idrissi, Porosity evaluation of protective coatings onto steel, through electrochemical techniques, Surf. Coat. Technol. 130 (2000) 224–232.
- [52] L. Li, K.P. Doran, G.M. Swain, Electrochemical characterization of trivalent chromium process (TCP) coatings on aluminum alloys 6061 and 7075, J. Electrochem. Soc. 160 (2013) C396–C401.